IOPscience iopscience.iop.org

Home Search Collections Journals About Contact us My IOPscience

Ultrahigh tunnel magnetoresistance using an artificial superlattice barrier with copper and aluminum oxide

This content has been downloaded from IOPscience. Please scroll down to see the full text.

2015 EPL 111 47005

(http://iopscience.iop.org/0295-5075/111/4/47005)

View the table of contents for this issue, or go to the journal homepage for more

Download details:

IP Address: 140.112.26.39
This content was downloaded on 11/11/2015 at 00:36

Please note that terms and conditions apply.

A Letters Journal Exploring the Frontiers of Physics

August 2015

EPL, **111** (2015) 47005 www.epljournal.org
doi: 10.1209/0295-5075/111/47005

Ultrahigh tunnel magnetoresistance using an artificial superlattice barrier with copper and aluminum oxide

Chang Hung Chen, Yu Hsiang Cheng and Wen Jeng Hsueh[(a)]

Nanoelectronics group, Department of Engineering Science and Ocean Engineering National Taiwan University 1, Sec. 4, Roosevelt Road, Taipei, 10660, Taiwan

received 10 March 2015; accepted in final form 17 August 2015
published online 4 September 2015

PACS 75.47.De – Giant magnetoresistance
PACS 75.70.Cn – Magnetic properties of interfaces (multilayers, superlattices, heterostructures)
PACS 73.40.Gk – Tunneling

Abstract – This paper proposes an ultrahigh tunnel magnetoresistance that is achieved by a magnetic tunnel junction with an artificial superlattice barrier that is composed of alternate layers of copper and aluminium oxide. By designing proper thickness filling factor of the superlattice barrier, ultrahigh magnetoresistance can be achieved. The tunnel magnetoresistance increases as the number of cells in the superlattice barrier increases. This ultrahigh magnetoresistance effect is attributed to the crystalline property of superlattices, similarly to the high magnetoresistance effect achieved by traditional crystalline MgO. There are more adjustable parameters, such as the lattice constant and the barrier height, in the artificial superlattice barrier than in a traditional crystalline-MgO barrier. This ultrahigh magnetoresistance effect may be used to design spintronic devices.

Copyright © EPLA, 2015

Introduction. – Tunnel magnetoresistance in magnetic tunnel junctions plays an important role in devices such as magnetoresistive random access memories, magnetic sensors and novel programmable logic gates. Improving the tunnel magnetoresistance (TMR) of magnetic tunnel junctions (MTJs) has always been an important issue [1–5]. Traditional MTJs with an amorphous aluminum oxide (Al-O) barrier, which have been widely studied for device applications, exhibit a TMR ratio up to 70% [6]. A large TMR ratio results if the amorphous Al-O barrier is replaced with crystalline MgO. Theoretical studies first predicted a TMR of more than 1000% in Fe/MgO/Fe systems [7,8]. In 2004, Yuasa *et al.* and Parkin *et al.* independently showed that the TMR ratio of Fe/MgO/Fe systems can be as much as 180% at room temperature [1,2]. This provides important evidence that crystalline material is key to improving the TMR ratio. Most recently, a large magnetoresistive effect has been accomplished because of a spin blockade in one-dimensional electron transport [3,9]. This generic feature allows the effect to be exploited in a broad range of one-dimensional systems.

As well as the ferromagnet-insulator-ferromagnet (FM-I-FM) tunnel junction, many studies have focused on the tunnel junction with a non-magnetic metal layer (N) inserted, since it has more interesting physics [10–19]. Even though the geometry of the FM-N-I-FM tunnel junction is merely a FM-I-FM tunneling junction with the N layer inserted, the inserted N layer results in different TMR phenomena, such as TMR oscillation as a function of the thickness of layer N [11,20]. This phenomenon is related to the quantum-well states that are formed in non-magnetic metals and to the resonant tunneling mechanism throughout the entire system. Coherent tunneling has been proven to be crucial to a large TMR. Both theoretical and experimental studies have shown that inserting non-magnetic metals into a MTJ is one of the easiest ways to ensure coherent tunneling [11,21].

Superlattices, a human-made material, may allow a higher MR ratio, since there are many adjustable parameters in superlattices, such as the lattice constant and the barrier height. The band structure of the superlattice can be tailored to different applications. It is well known that superlattices control the propagation of particles such as electron, photon, phonon and magnon very well [22–25]. However, superlattices are rarely used as a barrier in a MTJ. In our previous paper [9], the concept of using superlattice barrier (SLB) in MTJ is first proposed. The superlattice barrier is considered as the composition

(a) E-mail: hsuehwj@ntu.edu.tw

of non-magnetic metal and insulator. However, the properties of materials have not been considered in the previous study. In this work, parameters with realistic materials, such as copper, Al-O and cobalt, are adopted in the calculation to get more useful results. Moreover, the effect of thicknesses ratio of the superlattices on TMR ratio is studied. Compared to the previous work modulating only the thickness of non-magnetic metal, higher TMR ratio is achieved by modulating the thickness ratio of the superlattices in this work.

Model and formulation. – The Slonczewski model has been widely used to determine the magnetic properties of nano-systems [26]. Recently, this simple model has accurately described the TMR effect in a ferromagnet/insulator/ferromagnet (FM/I/FM) MTJ [27]. The same model is used to determine the TMR effect for a superlattice barrier MTJ:

$$H = \left(-\frac{\hbar^2}{2m}\nabla^2 + U - \vec{h}\cdot\vec{\sigma}\right), \tag{1}$$

where $\vec{h}$ is the molecular field [26], $\vec{\sigma}$ is the Pauli spin operator and U is the potential barrier height. It is assumed that the effective masses of the tunneling electrons in the insulator are the free electron masses as it is in the ferromagnetic electrodes. The fixed magnetization direction of the left-hand side electrode is the same as that of the quantization axis. Although $k_{||}$ is neglected in these notations, the effect of summation over $k_{||}$ is considered in the calculations. The tunnel current is calculated using the Landauer-Buttiker formula [28,29]

$$J^\sigma = \frac{e}{h}\int_{-\infty}^{\infty}\left[T^\sigma(E,V)\left\{f_{\mathrm{L}}(E,V) - f_{\mathrm{R}}(E,V)\right\}\right]\mathrm{d}E, \tag{2}$$

where T is the transmission coefficient, which can be obtained by the transfer matrix method.

The total current density is the sum of the current due to spin-up and spin-down electrons: $J = J^\uparrow + J^\downarrow$. The TMR is defined as $\mathrm{TMR} = (J_{\mathrm{P}} - J_{\mathrm{AP}})/J_{\mathrm{AP}}$, where J_{P} and J_{AP} are the current densities for the parallel and the anti-parallel configurations, respectively. The band structure of the magnetic tunnel junction with a SLB is determined using the periodic boundary. Floquet's theorem states that wave functions in a system with a periodic boundary must obey the Bloch waves. If the Bloch wave number, K, is complex, the Bloch wave is evanescent when it propagates in the system. The forbidden gap is given by the condition $|\cos(KL)| > 1$. However, if K is a real value, the Bloch wave is allowed to propagate in the system. The allowed band occurs if $|\cos(KL)| < 1$.

Results and discussion. – For a one-dimensional finite SLB that is enclosed by two ferromagnetic electrodes: $\mathrm{Co/(Cu/Al\text{-}O)}^n\mathrm{/Co}$, where n is the number of cells in the SLB, a small bias is applied between the two ferromagnetic electrodes. For cobalt, the magnitude of the molecular field, and the Fermi energy are $\Delta = 1.45\,\mathrm{eV}$ and

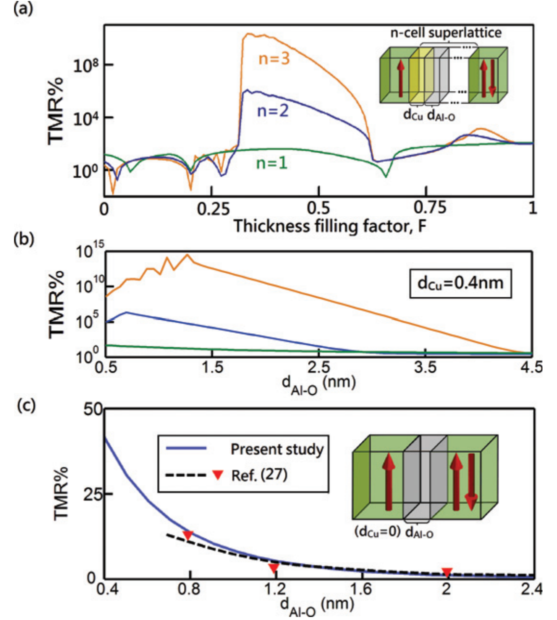

Fig. 1: (Color online) TMR ratio of the SLB MTJ and the single barrier MTJ. (a) The TMR ratio as a function of the thickness filling factor, F, for $n = 1$ (green line), $n = 2$ (blue line) and $n = 3$ (orange line), respectively. Inset: a sketch diagram of the n-cell SLB MTJ. The cobalt, copper, and Al-O layer are colored green, yellow and gray, respectively. (b) The TMR ratio as a function of the thickness of the Al-O barrier for $d_{\mathrm{Cu}} = 0.4\,\mathrm{nm}$. (c) The TMR ratio as a function of the thickness of the Al-O barrier in the Co/Al-O/Co structure. Inset: a sketch diagram of the Co/Al-O/Co structure. The dashed line and the inverted triangle respectively indicate the theoretical and experimental results in the reference.

$E_{\mathrm{F}} = 2.2\,\mathrm{eV}$, respectively. The barrier height for the Al-O layer is 1.6 eV [27]. The layers in the SLB are perpendicular to the x-axis. The TMR ratio of the SLB MTJ as a function of the thickness of the thickness filling factor, defined as $F = d_{\mathrm{Cu}}/(d_{\mathrm{Cu}} + d_{\mathrm{Al\text{-}O}})$, is shown in fig. 1(a). The sum of d_{Cu} and $d_{\mathrm{Al\text{-}O}}$ is 1 nm in the calculation. Oscillation of the TMR ratio is observed for varying the thickness filling factor. It is to be expected that this oscillation is related to the quantum-well states that are formed in non-magnetic metals and to the resonant tunneling mechanism that exists throughout the entire system [21]. When d_{Cu} is zero, the structure is reduced to a traditional FM/I/FM structure. On the other hand, it could be interesting to examine the effect of the change of the barrier thickness on the TMR keeping the thickness of the metallic layers constant, as shown in fig. 1(b). For $n = 1$, the TMR decreases monotonically for increasing barrier thickness. For $n = 2$ and $n = 3$, the TMR increases gradually for small barrier thickness and decreases gradually after reaching TMR maximum. Figure 1(c) shows the TMR ratio as a function of barrier thickness for the Co/Al-O/Co structure. As seen in fig. 1(c), the TMR ratio decreases as the barrier thickness increases. This result is consistent with both experimental and theoretical results in ref. [27]. In

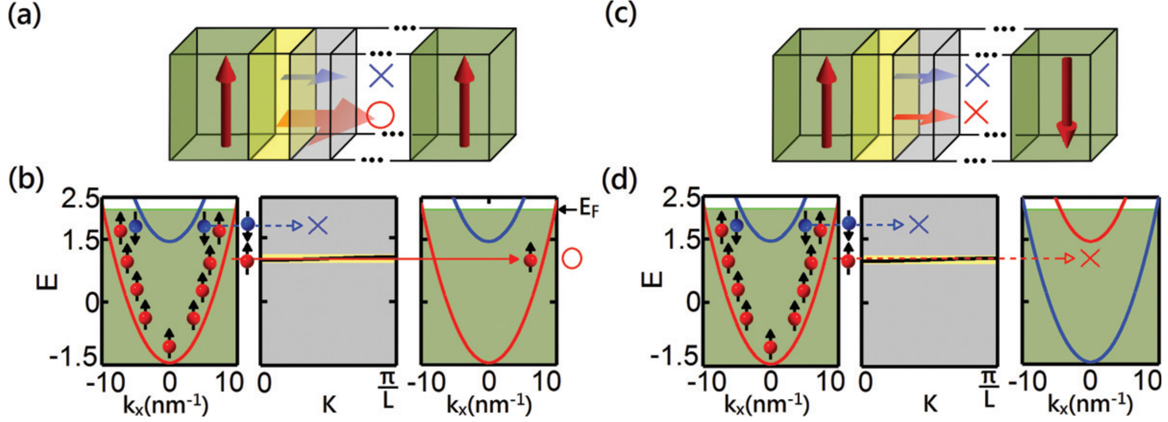

Fig. 2: (Color online) Sketch diagram and band structure of the SLB MTJ. Sketch diagram for current flow in a SLB MTJ in (a) parallel configuration and (c) anti-parallel configuration. The thickness filling factor is $F = 0.4$, for a large TMR, as shown in fig. 1. The spin-up and spin-down current flow in the SLB are represented by the light red and blue arrows that point toward the right electrode. The symbol × (∘) indicates that the transport of the electron is forbidden (allowed) in the SLB. The dispersion relation for a MTJ with a SLB in (b) parallel configuration and (d) anti-parallel configuration. The allowed (forbidden) band is colored yellow (gray).

fig. 1(a), TMR is large for certain thickness filling factor. The TMR ratio increases as n increases. Most importantly, this TMR ratio is orders of magnitude larger than that without copper. Therefore, band structure formed by the Cu/Al-O superlattice plays a key role in a higher TMR ratio.

In order to understand how the TMR ratio is enhanced by the band structure of the superlattice, figs. 2(a) and (b) show the sketch diagram and dispersion relation for a MTJ with a one-dimensional Cu/Al-O superlattice in parallel configuration. The thicknesses filling factor is $F = 0.4$. Therefore, the thicknesses of Cu and Al-O are 0.4 nm and 0.6 nm, respectively. Such thin thicknesses have been realized in the experiments [11,30]. In this configuration, only spin-up electrons are transmitted. Spin-down electrons cannot be transmitted because of the bandgap that is formed by the Cu/Al-O superlattice. Therefore, the current in this configuration is dominated by the contribution of the tunneling of spin-up electrons. Figures 1(c) and (d) show the sketch diagram and the dispersion relation for a MTJ with a SLB in anti-parallel configuration. In this configuration, both spin-up electrons and spin-down electrons cannot be transmitted, because of the bandgap that is formed by the SLB. Therefore, the current in the anti-parallel configuration, J_{AP}, is extremely small in a finite SLB MTJ. Since the definition of the TMR is $\mathrm{TMR} = (J_{\mathrm{P}} - J_{\mathrm{AP}})/J_{\mathrm{AP}}$, the TMR ratio is large, because of the suppression of current in the anti-parallel configuration. Analogous to the crystalline effect for MgO, crystalline superlattices an alternative way of achieving higher TMR ratio.

In order to understand this ultrahigh TMR, the transmission spectra for the MTJ with a SLB in the parallel configuration are shown in fig. 3(a) and fig. 3(b) for spin-up electrons and spin-down electrons, respectively. The thickness filling factor is $F = 0.4$. It is found that the

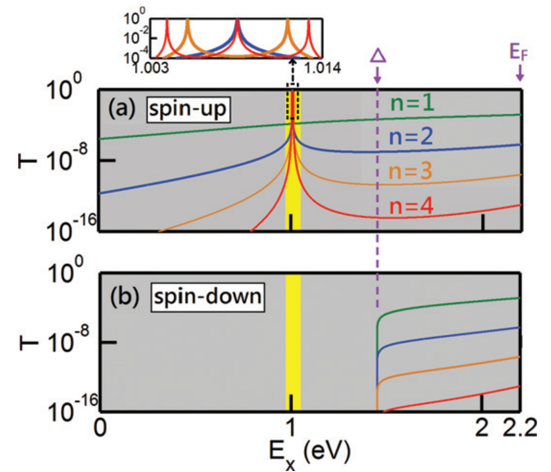

Fig. 3: (Color online) Transmission spectra in parallel configuration of the SLB MTJ. Transmission spectra for the $\mathrm{Co/(Cu/Al\text{-}O)}^n\mathrm{/Co}$ structure in parallel configuration, for (a) spin-up and (b) spin-down electrons. The green, blue, orange and red lines denote the $n = 1$, 2, 3 and 4 structures, respectively. The thickness filling factor is 0.4. The magnitude of molecular field for cobalt is $\Delta = 1.45\,\mathrm{eV}$.

spin-up electrons are transmitted via resonant tunneling, for $n > 1$ structures. For $n = 2$, there is only one resonant peak. For $n > 2$, splitting of the resonance states can be observed. For $n = 4$ (system with three quantum wells), there are three resonant peaks. For $n = 1$, resonant tunneling is not observed, since the structure is merely a single barrier structure. The resonant tunneling energy is within the allowed band. In the forbidden band, the transmittance decreases as n increases. For spin-down electrons, only the electrons within the energy range (Δ, E_{F}) can tunnel through the SLB. However, this energy range is fully covered by the bandgap. The transmission

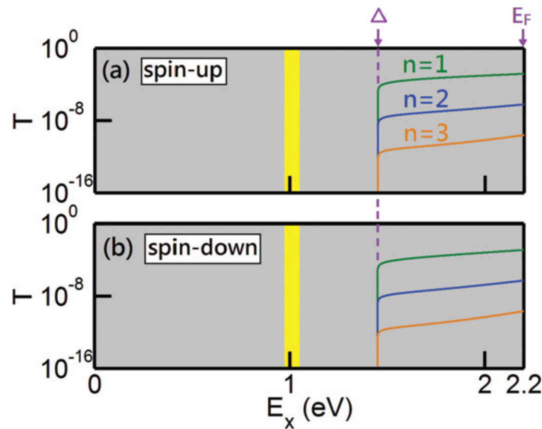

Fig. 4: (Color online) Transmission spectra in anti-parallel configuration of the SLB MTJ. Transmission spectra for the Co/(Cu/Al-O)^n/Co structure in anti-parallel configuration, for (a) spin-up and (b) spin-down electrons. The green, blue and orange lines denote the $n = 1$, 2 and 3 structures, respectively. The thickness filling factor is 0.4.

probability decreases significantly as n increases. For the $n = 3$ structure, the magnitude of the transmission probability is about 10^{-12}, so the current that is contributed by spin-down electrons is suppressed by the bandgap that is formed by the SLB. Therefore, the current in the parallel configuration, J_{P}, is mainly due to spin-up electrons within the allowed band. For the anti-parallel configuration, the transmission spectra of the MTJ with a n-cell SLB are shown in fig. 4(a) and fig. 4(b), for spin-up electrons and spin-down electrons, respectively. It is seen that the energy range (Δ, E_{F}), where spin-up and spin-down electrons can tunnel through the SLBs, is fully covered by the bandgap. Therefore, neither spin-up nor spin-down electrons can be transmitted in the anti-parallel configuration. In other words, the current in the anti-parallel configuration, J_{AP}, is suppressed by the bandgap of the SLB. This discussion shows that the current in the parallel configuration is due to the spin-up electrons and that in the anti-parallel configuration is due to neither spin-up electrons nor spin-down electrons. Therefore, the TMR ratio, defined as $(J_{\mathrm{P}} - J_{\mathrm{AP}})/J_{\mathrm{AP}}$, is large, since J_{AP} is quite small. However, this situation only occurs when there is a proper thickness filling factor.

In this work, we found that the TMR ratio of the MTJ with an artificial SLB, which can be both crystalline and one-dimensional, is strongly enhanced. In contrast to traditional crystalline-MgO barrier, there are more adjustable parameters in the artificial SLB, such as lattice constant and barrier height.

When the band structure of the SLB are properly designed, both spin-up and spin-down electrons are not allowed to transport in anti-parallel configuration. Introducing the band structure engineering of superlattice into the field of MTJ opens up a new way of achieving ultrahigh TMR ratio.

* * *

The authors acknowledge the support provided by the Ministry of Science and Technology of Taiwan, under grant Nos. MOST 103-3113-E-002-001 and MOST 103-2221-E-002-118.

REFERENCES

[1] Parkin S. S. P., Kaiser C., Panchula A., Rice P. M., Hughes B., Samant M. and Yang S. H., *Nat. Mater.*, **3** (2004) 862.
[2] Yuasa S., Nagahama T., Fukushima A., Suzuki Y. and Ando K., *Nat. Mater.*, **3** (2004) 868.
[3] Mahato R. N., Lülf H., Siekman M. H., Kersten S. P., Bobbert P. A., De Jong M. P., De Cola L. and Van Der Wiel W. G., *Science*, **341** (2013) 257.
[4] Fullerton E. E. and Schuller I. K., *ACS Nano*, **1** (2007) 384.
[5] Lekshmi I. C., Buonsanti R., Nobile C., Rinaldi R., Cozzoli P. D. and Maruccio G., *ACS Nano*, **5** (2011) 1731.
[6] Dexin W., Nordman C., Daughton J. M., Zhenghong Q. and Fink J., *IEEE Trans. Magn.*, **40** (2004) 2269.
[7] Mathon J. and Umerski A., *Phys. Rev. B*, **63** (2001) 220403.
[8] Butler W. H., Zhang X. G., Schulthess T. C. and MacLaren J. M., *Phys. Rev. B*, **63** (2001) 054416.
[9] Chen C. H. and Hsueh W. J., *Appl. Phys. Lett.*, **104** (2014) 042405.
[10] Moodera J. S., Nowak J., Kinder L. R., Tedrow P. M., Van De Veerdonk R. J. M., Smits B. A., Van Kampen M., Swagten H. J. M. and De Jonge W. J. M., *Phys. Rev. Lett.*, **83** (1999) 3029.
[11] Yuasa S., Nagahama T. and Suzuki Y., *Science*, **297** (2002) 234.
[12] Yuasa S., Fukushima A., Kubota H., Suzuki Y. and Ando K., *Appl. Phys. Lett.*, **89** (2006) 042505.
[13] Matsumoto R., Fukushima A., Yakushiji K., Nishioka S., Nagahama T., Katayama T., Suzuki Y., Ando K. and Yuasa S., *Phys. Rev. B*, **79** (2009) 174436.
[14] LeClair P., Swagten H. J. M., Kohlhepp J. T., Van De Veerdonk R. J. M. and De Jonge W. J. M., *Phys. Rev. Lett.*, **84** (2000) 2933.
[15] Greullet F., Tiusan C., Montaigne F., Hehn M., Halley D., Bengone O., Bowen M. and Weber W., *Phys. Rev. Lett.*, **99** (2007) 187202.
[16] Itoh H., Inoue J., Umerski A. and Mathon J., *Phys. Rev. B*, **68** (2003) 174421.
[17] Zhang S. and Levy P. M., *Phys. Rev. Lett.*, **81** (1998) 5660.
[18] Yang J., Wang J., Zheng Z. M., Xing D. Y. and Chang C. R., *Phys. Rev. B*, **71** (2005) 214434.
[19] Ziu Z. P., Fang Z. B., Yang J. and Xing D. Y., *Phys. Rev. B*, **73** (2007) 014432.
[20] Wilczynski M. and Barnas J., *J. Magn. & Magn. Mater.*, **221** (2000) 373.
[21] Choi C. and Lee B. C., *Phys. Rev. B*, **86** (2012) 134411.
[22] Cheng Y. H., Chang C. H., Chen C. H. and Hsueh W. J., *Phys. Rev. A*, **90** (2014) 023830.
[23] Tsu R. and Esaki L., *Appl. Phys. Lett.*, **22** (1973) 562.

[24] Macfarlane R. J., Jones M. R., Lee B., Auyeung E. and Mirkin C. A., *Science*, **341** (2013) 1222.
[25] Hsueh W. J., Chen C. T. and Chen C. H., *Phys. Rev. A*, **78** (2008) 013836.
[26] Slonczewski J. C., *Phys. Rev. B*, **39** (1989) 6995.
[27] Yanik A. A., Klimeck G. and Datta S., *Phys. Rev. B*, **76** (2007) 045213.
[28] Kim W. Y. and Kim K. S., *Nat. Nanotechnol.*, **3** (2008) 408.
[29] Datta S., *Electronic Transport in Mesoscopic Systems* (Cambridge University Press) 1997.
[30] Santos T. S., Lee J. S., Migdal P., Lekshmi I. C., Satpati B. and Moodera J. S., *Phys. Rev. Lett.*, **98** (2007) 016601.